Chinese Chemical Letters 33 (2022) 466–469

Contents lists available at ScienceDirect

Chinese Chemical Letters

journal homepage: www.elsevier.com/locate/cclet

A benzo[*ghi*]-perylene triimide based double-cable conjugated polymer for single-component organic solar cells

Dan Wang[a,b,1], Zhaofan Yang[b,1], Feng Liu[a,c,*], Chengyi Xiao[b], Yonggang Wu[a,*], Weiwei Li[b,*]

[a] College of Chemistry and Environmental Science, Hebei University, Baoding 071002, China
[b] Beijing Advanced Innovation Center for Soft Matter Science and Engineering & State Key Laboratory of Organic-Inorganic Composites, Beijing University of Chemical Technology, Beijing 100029, China
[c] College of Basic Medicine, Hebei University, Baoding 071002, China

ARTICLE INFO

Article history:
Received 12 May 2021
Revised 31 May 2021
Accepted 15 June 2021
Available online 25 June 2021

Keywords:
Double-cable polymer
Single-component organic solar cells
BPTI
Electron withdrawing
Electron transporting channels

ABSTRACT

Single-component organic solar cells (SCOSCs) with high stability and simplified fabrication process are supposed to accelerate the commercialization of organic photovoltaics. However, the types of photo-active materials and photovoltaic performance of SCOSCs are still far lagging behind the bulk-heterojunction type organic solar cells (BHJ OSCs). It is still an arduous task to introduce new photo-active materials into SCOSCs, aiming to improve the efficiencies of SCOSCs. One feasible way is to construct double-cable polymers with new structures and tune conformation, morphology and mobility for the improvement in power conversion efficiencies (PCEs). Hence, in this work, we constructed a new double-cable polymer PBTT-BPTI by introducing fused core 5,7-dibromo-2,3-bis(2-ethylhexyl)benzo[1,2-*b*:4,5-*c*']dithiophene-4,8-dione (TTDO) into the main backbone and benzo[*ghi*]-perylene triimide (BPTI) unit into the side chain. Both of the two units show strong electron-withdrawing property, which are expected to broaden absorption spectra and enhance intermolecular interaction. The double-cable polymer exhibited a broad absorption in the range of 300-700 nm with an optical band gap (E_g) of 1.79 eV. The PCE of PBTT-BPTI-based SCOSCs was 2.15%, which may be limited by the unconstructed efficient electron transporting channels.

Organic solar cells (OSCs) have attracted tremendous attention due to their advantages of low-cost, solution-processing and large-scale application [1–11]. Nowadays, most attentions have focused on the bulk-heterojunction (BHJ) type OSCs, which consist of donor and acceptor in the photo-active layers and have achieved the highest power conversion efficiencies (PCEs) over 18% [12–17]. However, the BHJ-type OSCs may encounter some issues in the commercialization process, such as long-term stability, unstable phase separation and cost [18–27]. The single-component organic solar cells (SCOSCs), with one conjugated material as photo-active layer, can simplify the fabrication process and solve the self-aggregation issues for improved stability [28–33]. Hence, SCOSCs are one of promising candidates for commercial applications of OSCs in the future.

The champion PCE of SCOSCs has reached 8.40% [34], which is still far lagging behind the PCEs of BHJ type OSCs. This is mainly due to the limited types of single-component conjugated materials [35]. Therefore, more efforts are still needed to be devoted into designing and synthesizing of new photo-active materials for high-performance SCOSCs. Many types of materials have been reported for the applications in SCOSCs, such as block copolymers [36], double-cable conjugated polymers [37] and molecular dyads [38]. Double-cable conjugated polymers as one type of the photo-active materials used in SCOSCs, are usually constructed by donor-acceptor conjugated polymers as conjugated backbone and small molecular acceptors as side chain [39–42]. Both conjugated backbones and side units can significantly influence the PCEs of SCOSCs through the molecular packing, cooperative crystallization, miscibility, *etc.*

The benzo[*ghi*]-perylene triimide (BPTI) unit, which has larger π-conjugated structure than the naphthalene diimides (NDI) or perylene bisimides (PBI) acceptors, was used to construct a double-cable polymer PTPDBPTI in our previous report [43]. The BPTI unit effectively tuned the aggregation/crystallization of PTPDBPTI polymers and was able to construct effective electron transporting channels, thus balancing hole and electron mobilities. The PCEs of SCOSCs were promoted from 1.92% to 4.34% when replac-

* Corresponding authors.
E-mail addresses: liufeng@hbu.edu.cn (F. Liu), wuyonggang@hbu.edu.cn (Y. Wu), liweiwei@iccas.ac.cn (W. Li).
[1] These authors contribute equally to this work.

https://doi.org/10.1016/j.cclet.2021.06.042
1001-8417/

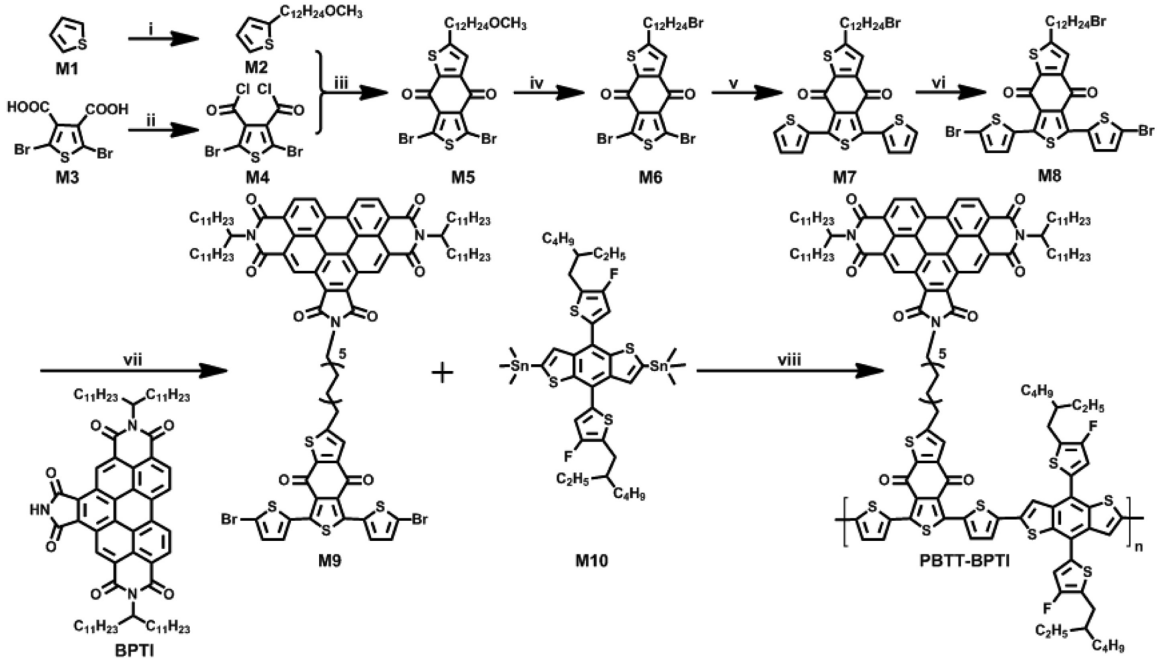

Scheme 1. Synthetic routes for the monomers and the double-cable polymer PBTT-BPTI. (i) *n*-BuLi, -78 °C, 3 h, 1,12-dibromodecane, THF, 50 °C, 4-6 h; (ii) Oxalyl chloride, CH_2Cl_2, 0 °C, overnight; (iii) $AlCl_3$, $ClCH_2CH_2Cl$, 0 °C, overnight; (iv) HBr, reflux, overnight; (v) $Pd_2(dba)_3$, $[(t\text{-}Bu)_3PH]BF_4$, K_3PO_4(aq) in THF, N_2, 80 °C, 7 h; (vi) NBS, 0 °C, N_2, overnight; (vii) K_2CO_3, DMF, 80 °C, N_2, overnight; (viii) $Pd(PPh_3)_4$, toluene, N_2, 115 °C, 13 h.

ing the PBI side units by BPTI units. Hence, the BPTI unit can act as a new electron-deficient side unit in double-cable polymers. The conjugated units in conjugated backbone of double-cable polymers can also significantly influence the photovoltaic property of SCOSCs. He *et al*. reported a new donor material PBTT-F, with fused core 5,7-dibromo-2,3-bis(2-ethylhexyl)benzo[1,2-*b*:4,5-*c*']dithiophene-4,8-dione (TTDO) as conjugated unit [44]. The strong electron-withdrawing property of TTDO core is beneficial to extend the absorption spectra and enhance the intramolecular charge transfer, leading to the improved photovoltaic performance of PBTT-F/Y6 based NFOSCs with an outstanding PCE of 16.1%.

Inspiring by the above work, we developed a new double-cable conjugated polymer PBTT-BPTI by introducing TTDO to the main backbone and BPTI as the side unit in this work. The electron-withdrawing property of the TTDO unit significantly broadens the absorption spectra, and both TTDO unit and BPTI unit affect the aggregation properties of double-cable polymers. The SCOSCs based on the double-cable polymer PBTT-BPTI exhibited a PCE of 2.15% after the optimization of post annealing and solvents.

The synthetic routes for the monomers and the double-cable polymer PBTT-BPTI were presented in Scheme 1 and the details were shown in Supporting information. The monomer **M9** was synthesized *via* the monomer **M8** and BPTI unit. Then, the monomer **M9** and **M10** were used to perform *Stille* polymerization to yield the double-cable polymer PBTT-BPTI. The molecular weight of PBTT-BPTI was determined by high temperature gel permeation chromatography (GPC) with trichlorobenzene (TCB) as eluent at 150 °C. The number-average molecular weights (M_n) and polydispersity indices ($Đ$) of PBTT-BPTI were 57.10 kg/mol and 3.70, respectively. The double-cable polymer showed good solubility in *o*-DCB (1,2-dichlorobenzene) and high thermal stability (Fig. S1 in Supporting information) with decomposition temperature of 375 °C. The differential scanning calorimetry (DSC) measurement showed that the double-cable conjugated polymer PBTT-BPTI has no thermal transition in the range of measured temperature (Fig. S2 in Supporting information).

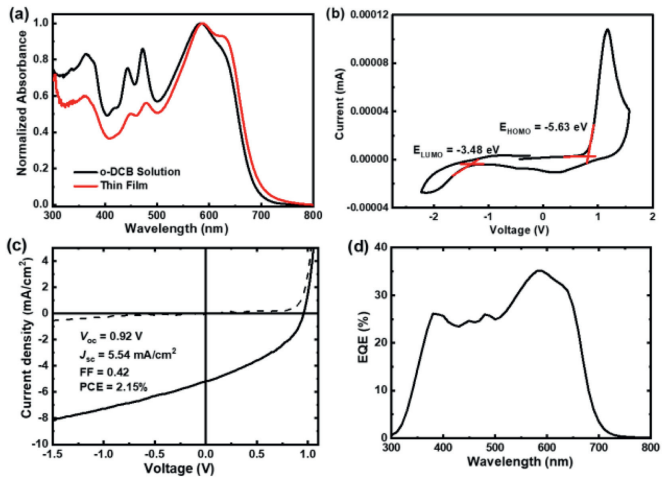

Fig. 1. (a) UV-vis absorption spectra of the double-cable polymer PBTT-BPTI in *o*-DCB solution and thin film. (b) HOMO/LUMO energy levels determined from cyclic voltammetry measurements (*vs.* Fc/Fc^+). (c) *J*–*V* characteristics of the optimized PBTT-BPTI-based SCOSCs. (d) EQE spectrum of the optimized PBTT-BPTI-based SCOSCs.

The UV-vis absorption spectra of PBTT-BPTI in *o*-DCB solution and thin film are present in Fig. 1a. The double-cable polymer PBTT-BPTI shows a broad absorption in the range of 300-700 nm in *o*-DCB solution. The absorption peaks at 363, 417, 442 and 473 nm are contributed to the BPTI unit in the side chain [43, 45]. Three absorption peaks of BPTI unit at λ = 417, 442 and 473 nm are assigned to the S_0 to S_1 transition energy, which is along the long-axis direction. And the absorption peak in the range of 350-400 nm is assigned to the S_0 to S_2 transition energy, which is along the short-axis direction [45]. The absorption peak at 584 nm in the range of 500-700 nm is contributed to the typical characteristic of PBTT conjugated backbone, and the shoulder peak implies the presence of molecular preaggregation in solution [46]. The ab-

Table 1
Characteristics of SCOSCs based on PBTT-BPTI. The thickness is ~50 nm for these films.

Solvent	Annealing temperature (°C)	J_{sc} (mA/cm^2)	V_{oc} (V)	FF	PCE (%)
o-DCB/DIO (1%)	r.t.	5.18	0.96	0.39	1.95
o-DCB/DIO (1%)	150	5.12	0.94	0.42	2.03
o-DCB/DIO (1%)	200	5.54	0.92	0.42	2.15
o-DCB/DIO (1%)	230	5.23	0.90	0.40	1.87
o-DCB	200	5.53	0.86	0.38	1.80
o-DCB/DIO (0.5%)	200	5.36	0.88	0.41	1.93
o-DCB/DIO (1%)	200	5.54	0.92	0.42	2.15
o-DCB/DIO (2%)	200	5.36	0.91	0.40	1.98

sorption spectra of PBTT-BPTI in thin films showed a slightly red-shifted absorption peak at 587 nm and an obvious shoulder compared to that in solution, indicating strong aggregation of polymer backbones and intermolecular π–π interaction in the solid state. Interestingly, the polymer PBTT-BPTI shows the similar absorption spectra in solution and in thin film, but the absorption intensities of peaks are quite different, which may be due to the different degree of aggregation of BPTI unit and PBTT unit. The conjugated backbone exhibited stronger aggregation property than the BPTI side unit, which may lead to unbalanced charge transport and further decrease photovoltaic performance in SCOSCs. The optical band gaps (E_gs) in solution and in thin film are 1.80 eV and 1.79 eV, respectively. Cyclic voltammogram (CV) curve of PBTT-BPTI in acetonitrile that contained 1.0 mol/L NBu_4PF_6 is shown in Fig. 1b. The highest occupied molecular orbital (HOMO) level of PBTT-BPTI is −5.63 eV and the lowest unoccupied molecular orbital (LUMO) is −3.48 eV, respectively, implying that the LUMO level of PBTT-BPTI is similar to the BPTI side unit [43].

PBTT-BPTI was then used to fabricate SCOSCs with an inverted configuration of ITO/ZnO/PBTT-BPTI/MoO_3/Ag. The fabrication conditions, including the optimization of additive content and annealing temperature, were applied to achieve the best device performance (Table 1). The optimized *J-V* characteristics and external quantum efficiency (EQE) curve are presented in Figs. 1c and d. The PBTT-BPTI-based SCOSCs achieved the best PCE of 2.15% with a short-circuit current density (J_{sc}) of 5.54 mA/cm^2, open-circuit voltage (V_{oc}) of 0.92 V and fill factor (FF) of 0.42, in which the photo-active layer with the thickness of 50 nm was fabricated from *o*-DCB with 1% DIO, thermal-annealed at 200 °C for 10 min. The low J_{sc} may be attributed to the unbalanced charge transport based on different aggregation properties between conjugated backbone and the pendant unit in the side chain. Fig. 1d showed the EQE spectra for the best device. The PBTT-BPTI-based SCOSCs exhibited a broad response range (300-750 nm). The integral J_{sc}^{EQE} calculated from EQE curve agrees well with the observed J_{sc} in the *J-V* measurement, with a mismatch within 5%. Space–charge limited current (SCLC) measurement was applied to study the charge transport properties of PBTT-BPTI-based SCOSCs (Fig. S3 in Supporting information). Unfortunately, we failed to obtain the electron mobility of the SCOSCs and the hole mobility was 2.06 × 10^{-4} cm^2 V^{-1} s^{-1}, indicating the unconstructed electron transporting channels.

The crystalline property of PBTT-BPTI was studied by atomic force microscopy (AFM) (Figs. 2a and b) and grazing-incidence wide-angle X-ray scattering (GIWAXS) measurement (Figs. 2c and d). The crystallographic parameters are summarized at Table S1 (Supporting information). As shown in Figs. 2a and b, thin film of PBTT-BPTI fabricated from *o*-DCB/DIO showed small domains on the surface with a low roughness of 0.87 nm. The GIWAXS patterns show a clear (100) diffraction peak in the in-plane direction and (010) diffraction peak in the out-of-plane direction for PBTT-BPTI thin film, indicating the face-on orientation. The high diffraction peaks also indicate the strong the aggregation/crystallization of double-cable polymer PBTT-BPTI, which would result in the unbalance charge transfer and hence lower the photovoltaic performance.

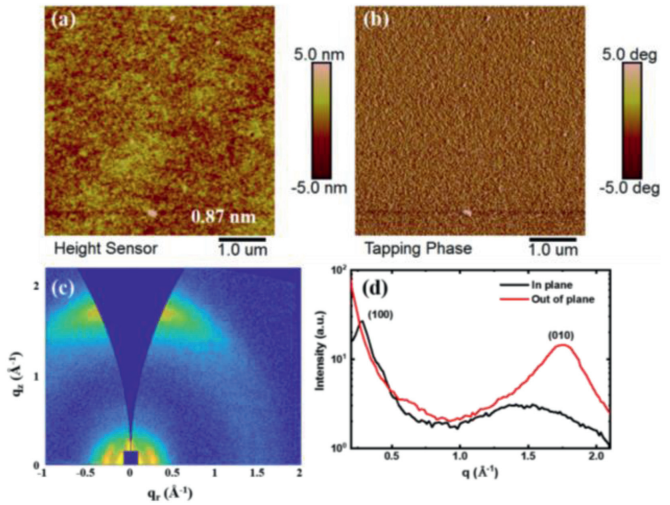

Fig. 2. AFM (a) height and (b) phase images (5 × 5 μm) of PBTT-BPTI thin film. Characteristics of the blended thin films spin-casted on Si substrates. (c) GIWAXS patterns, (d) the out-of-plane (OOP) and in-plane (IP) cuts of the corresponding GIWAXS patterns.

In summary, we have successfully introduced two electron-deficient units (BPTI and TTDO) into a new-constructed double-cable polymer PBTT-BPTI. The double-cable polymer PBTT-BPTI shows a board absorption spectra in the range of 300 nm to 700 nm with a low bandgap of 1.79 eV. However, the different aggregation properties between the PBTT main backbone and BPTI units led to the unbalanced charge transfer, resulting a low PCE of 2.15% for PBTT-BPTI-based SCOSCs. Our results provide a new material gallery for SCOSCs, and further demonstrate that the aggregation distinction between conjugated backbone and side units is a key parameter to influence the performance of the double-cable polymers based SCOSCs.

Declaration of competing interest

The authors declare that they have no known competing financial interests or personal relationships that could have appeared to influence the work reported in this paper.

Acknowledgmentss

This study is jointly supported by National Key R&D Program of China (Nos. 2018YFA0208504, 2017YFA0204702), National Natural Science Foundation of China (Nos. 51773207, 21574138, 21905018) and Natural Science Foundation of Hebei Province (No. B2020201032). This work was further supported by the Fundamental Research Funds for the Central Universities (No. XK1802-2) and

Open Project of State Key Laboratory of Supramolecular Structure and Materials (No. sklssm202043)

Supplementary materials

Supplementary material associated with this article can be found, in the online version, at doi:10.1016/j.cclet.2021.06.042.

References

[1] O. Inganäs, Adv. Mater. 30 (2018) 1800388.
[2] M. Riede, D. Spoltore, K. Leo, Adv. Energy Mater. 11 (2021) 2002653.
[3] Y.W. Li, G.Y. Xu, C.H. Cui, Y.F. Li, Adv. Energy Mater. 8 (2018) 1701791.
[4] K. Fukuda, K. Yu, T. Someya, Adv. Energy Mater. 10 (2020) 2000765.
[5] G. Jia, S. Zhang, L. Yang, et al., Acta Phys. Chim. Sin. 35 (2019) 76–83.
[6] B. Liu, Y. Xu, D. Xia, et al., Acta Phys. Chim. Sin. 37 (2021) 2009056.
[7] Y. Li, Y. Xu, F. Yang, et al., Chin. Chem. Lett. 30 (2019) 222–224.
[8] F. Liu, C. Li, J. Li, et al., Chin. Chem. Lett. 31 (2020) 865–868.
[9] N. Yan, C. Zhao, S. You, Y. Zhang, W. Li, Chin. Chem. Lett. 31 (2020) 643–653.
[10] X. Wang, A. Tang, J. Yang, et al., Sci. China Chem. 63 (2020) 1666–1674.
[11] A. Tang, W. Song, B. Xiao, et al., Chem. Mater. 31 (2019) 3941–3947.
[12] Q. Liu, Y. Jiang, K. Jin, et al., Sci. Bull. 65 (2020) 272.
[13] Y. Lin, Y. Firdaus, F.H. Isikgor, et al., ACS Energy Lett. 5 (2020) 2935–2944.
[14] C. Zhu, J. Yuan, F.F. Cai, et al., Energy Environ. Sci. 13 (2020) 2459–2466.
[15] M. Zhang, L. Zhu, G. Zhou, et al., Nat. Commun. 12 (2021) 309.
[16] K. Jin, Z. Xiao, L. Ding, J. Semicond. 42 (2021) 060502.
[17] Y. Chen, H. Chen, H. Guan, et al., Chin. Chem. Lett. 32 (2021) 229–233.
[18] W. Zheng, X. Luo, Y. Zhang, et al., ACS Appl Mater Interfaces 12 (2020) 23190–23198.
[19] L. Yao, N. Guijarro, F. Boudoire, et al., J. Am. Chem. Soc. 142 (2020) 7795–7802.
[20] J. Wu, Q. Fan, M. Xiong, et al., Nano Energy 82 (2020) 105679.
[21] S. Park, T. Kim, S. Yoon, et al., Adv. Mater. 32 (2020) 2002217.
[22] S. Feng, H. Lu, Z. Liu, et al., Acta Phys. Chim. Sin. 35 (2019) 355–360.
[23] Y. Guo, A. Zhang, C. Li, W. Li, D. Zhu, Chin. Chem. Lett. 29 (2018) 371–373.
[24] N. Wang, W. Yang, S. Li, et al., Chin. Chem. Lett. 30 (2019) 1277–1281.
[25] P. Yu, G. Feng, J. Li, et al., J. Mater. Chem. C 8 (2020) 2790–2797.
[26] C. Li, X. Wu, X. Sui, et al., Angew. Chem. Int. Ed. 58 (2019) 15532–15540.
[27] D. Xia, F. Yang, J. Li, C. Li, W. Li, Mater. Chem. Front. 3 (2019) 1565–1573.
[28] W. Lai, C. Li, J. Zhang, et al., Chem. Mater. 29 (2017) 7073–7077.
[29] V.D. Mitchell, D.J. Jones, Polym. Chem. 9 (2018) 795–814.
[30] G. Feng, J. Li, F.J.M. Colberts, et al., J. Am. Chem. Soc. 139 (2017) 18647–18656.
[31] G. Feng, J. Li, Y. He, et al., Joule 3 (2019) 1765–1781.
[32] Y. GENG, Acta Phys. Chim. Sin. 35 (2019) 1311–1312.
[33] C. Wang, F. Liu, Q.M. Chen, et al., Chin. J. Polym. Sci. 39 (2021) 525–536.
[34] X. Jiang, J. Yang, S. Karuthedath, et al., Angew. Chem. Int. Ed. 59 (2020) 21683–21692.
[35] D. Xia, C. Li, W. Li, Chem. Rec. 19 (2019) 962–972.
[36] S.H. Park, Y. Kim, N.Y. Kwon, et al., Adv. Sci. 7 (2020) 1902470.
[37] X. Jiang, J. Yang, S. Karuthedath, et al., Angew. Chem. Int. Ed. 59 (2020) 21683–21692.
[38] S. Lucas, J. Kammerer, M. Pfannmöller, et al., Sol. RRL 5 (2021) 2000653.
[39] S. Liang, Y. Xu, X. Jiang, C. Li, W. Li, Dyes Pigm. 170 (2019) 107575.
[40] D. Xia, F. Yang, J. Li, C. Li, W. Li, Mater. Chem. Front. 3 (2019) 1565–1573.
[41] S.J. Liang, Y.H. Xu, C. Li, et al., Polym. Chem. 10 (2019) 4584–4592.
[42] C. Li, X. Wu, X. Sui, et al., Angew. Chem. Int. Ed. 58 (2019) 15532–15540.
[43] F. Yang, J.Y. Li, C. Li, W.W. Li, Macromolecules 52 (2019) 3689–3696.
[44] P. Chao, H. Chen, Y. Zhu, et al., Adv. Mater. 32 (2020) 1907059.
[45] H.C. Chen, C.P. Hsu, J.N. Reek, R.M. Williams, A.M. Brouwer, ChemSusChem 8 (2015) 3639–3650.
[46] P. Chao, H. Chen, Y. Zhu, et al., Adv. Mater. 32 (2020) 1907059.